Grafting of Imidazolium Based Ionic Liquid on the Pore Surface of Nanoporous Materials—Study of Physicochemical and Thermodynamic Properties

Olga C. Vangeli,[†] George E. Romanos,*[,†] Konstantinos G. Beltsios,[‡] Demosthenes Fokas,[‡] Evangelos P. Kouvelos,[†] Konstantinos L. Stefanopoulos,[†] and Nick K. Kanellopoulos[†]

Institute of Physical Chemistry, National Center for Scientific Research Demokritos, Agia Paraskevi, Athens 153 10, Greece, and Department of Materials Science and Engineering, University of Ioannina, 45110 Ioannina, Greece

Received: December 28, 2009; Revised Manuscript Received: April 9, 2010

Supported ionic liquid phase (SILP) systems were prepared by immobilizing a methylimidazolium cation based ionic liquid onto the pore surface of two types of support, MCM-41 and Vycor. The "grafting to" method was applied, involving (3-chloropropyl)-trialkoxysilane anchoring on the supports' silanol groups, followed by treatment with 1-methylimidazole and ion exchange with PF_6^-. Optimum surface pretreatment procedures and reaction conditions for enhanced ionic liquid (IL) loading were properly defined and applied for all modifications. A study on the effect of different pore sizes on the physical state of the grafted 1-(silylpropyl)-3-methylimidazolium-hexafluorophosphate ([spmim][PF_6^-]) was also conducted. The [spmim][PF_6^-] crystallinity under extreme confinement in the pores was investigated by modulated differential scanning calorimetry (DSC) and X-ray diffraction (XRD) and was further related to the capacity of the developed SILP to preferentially adsorb CO_2 over CO. For this purpose, CO_2 and CO absorption measurements of the bulk ionic liquid [bmim][PF_6^-] and the synthesized alkoxysilyl-IL were initially performed at several temperatures. The results showed an enhancement of the bulk IL performance to preferentially adsorb CO_2 at 273 K. The DSC analysis of the SILPs revealed transition of the melting point of the grafted alkoxysilyl-IL to higher temperatures when the support pore size was below 4 nm. The 2.3 nm MCM-41 SILP system exhibited infinite CO_2/CO separation capacity at temperatures below and above the melting point of the bulk IL phase, adsorbing in parallel significant amounts of CO_2 in a reversible manner. These properties make the developed material an excellent candidate for CO_2/CO separation with pressure swing adsorption (PSA) techniques.

1. Introduction

Ionic liquids (ILs) are the subject of a large number of the research studies that are currently being conducted, due to their unique chemical and physical properties that bring about the potential of several interesting applications. Properties such as the negligible vapor pressure, thermal stability, unique solvation, good ion conductivity, catalytic activity, and selectivity performance make them excellent candidates as extraction media,[1] solvents for organic, organometallic synthesis and catalysis,[2,3] electrolytes, supports for the immobilization of enzymes and as materials for gas separation and purification technologies. Especially in the later case, any reliable information on the gas solubility in the IL phase is mandatory for the calculation of vapor/liquid equilibria occurring in separation processes or reaction systems. For this reason, recent studies on the interaction of ionic liquids with several gases primarily concern the accurate definition of solubility factors in the bulk liquid phase and at temperatures well above the IL melting point.[4−6] Among the several gas/IL pairs, the system carbon dioxide/[bmim][PF_6^-] has been extensively investigated by a considerable number of research groups,[4,7−10] using different experimental techniques, whereas the majority of the referred CO_2 solubility values are in good accordance within ±10%. Contrary, for the system CO/[bmim][PF_6^-], the encountered solubility values[11−13] deviate by more than 50%, whereas, in some cases,[14] the CO solubility is referred to as nondetectable. Regardless of the existent discrepancies, the gas solubility results foresee excellent capacity of some ionic liquids, e.g., [bmim][PF_6^-], to separate CO_2 from CO, an application of high importance in the production of synthesis gas. Carbon dioxide is a desirable feed to the reformer (or gasifier) reducing methane consumption and producing syngas with an optimum H_2/CO ratio. However, it can also be found in the reformer/gasifier discharge stream where it is undesirable and must be separated and recycled back to the feed. A prospect to render sustainable the CO_2/CO separation process with ILs is to stabilize them in the pore structure of membranes or porous solids, thus circumventing the problem of mass transport limitation and the need for high amounts of ILs. The latest developments in supported ionic liquid phase (SILP) systems are mainly focusing on catalytic applications by immobilizing a thin film of catalyst bearing ionic liquid onto a high surface area support. The SILP concept combines the advantages of homogeneous catalysis with heterogeneous process technology, and a variety of reactions have been studied where SILP catalysts proved to be more active and selective than common systems.[15−17] Ionic liquids are usually deposited by covalent bonding via ionic liquid fragments attached to the support[18] or by physisorption using conventional wet impregnation techniques.[19] A slightly different method for the immobilization of ionic liquids on silica supports is their confinement into the nanocavities of metal oxides during the sol−gel

* Corresponding author. E-mail: groman@chem.demokritos.gr.
[†] National Center for Scientific Research Demokritos.
[‡] University of Ioannina.

10.1021/jp912205y
Published on Web 04/22/2010

method.[20] A factor of great importance in all catalytic and separation processes is the stability of the supported ionic liquid phase, and the most promising results on this issue were obtained by the silica grafting method,[21,22] where alkoxysilyl imidazolium based ionic liquids are initially synthesized and then grafted to the support surface.

In this work, a different approach describable as the "grafting to" route is explored. We initially proceeded to silane anchoring on the supports' silanol groups and further to the treatment with 1-methylimidazole and ion exchange with PF_6^-. This sequential development was applied for two reasons: (a) bypassing of diffusion limitations in the reaction of a quite bulky alkoxysilyl ionic liquid molecule with the surface silanol groups and (b) availability of the option to examine the effects of support surface pretreatment (surface silanol group population) and silane grafting extent on the amount of the deposited IL phase. A series of acidic and basic hydrolysis procedures were applied for the pretreatment of the support surface, and the optimum conditions (pH, temperature, period) were determined through water vapor desorption experiments[23] and applied for all further modifications. Extended leaching of the materials under extremely strong acidic or basic conditions was detected by LN_2 adsorption experiments. Several parameters affecting the grafting reaction such as the solvent polarity, temperature, trace moisture, and silane concentration were tuned to the optimum for enhanced silane loading which was investigated with water vapor desorption, FTIR, and elemental analysis. Liquid nitrogen adsorption and SAXS gave insight on the morphological characteristics of the anchored silane phase.

Ionic liquid loading was in general analogous to silane loading except for the cases where extended polymerization of the silane on the support surface was observed. The thermal stability and physical state of the deposited ionic liquid were examined by TGA, DSC, and XRD analysis. In a recent study, a transition of the ionic liquid [bmim][PF_6^-] from liquid to high-melting-point crystal was observed when confined in multiwalled carbon nanotubes.[24] In addition, the coexistence of liquid and solid phases of [bmim][PF_6^-] liquid on mica surfaces at room temperature is also investigated.[25] On this concept, both the physical state of the ionic liquid under extreme confinement into the pores of mesoporous materials and its relation to the CO_2 and CO absorption capacity may be of great interest; to this end, gravimetric CO_2/CO absorption experiments were performed at temperatures above and below the melting point of [bmim][PF_6^-].

2. Experimental Section

2.1. Apparatuses and Measurements. The CO_2, CO gas solubility measurements and the water vapor adsorption−desorption experiments were performed with a gravimetric microbalance (IGA, Hiden Analytical). The masses of the sample and counterweight pans, the hooks, the counterweight material, and the hang chains of the microbalance assembly were of the order of 100−300 mg/item and were defined with an accuracy of ±0.1%. The materials were appropriately selected to induce a symmetrical configuration to the balance setup in order to minimize buoyancy effects. The microbalance had a 0.1 μg stable resolution. The amount of the bulk ionic liquid usually applied was 100−150 mg. Before each measurement, the bulk ionic liquid samples were degassed at 353 K and high vacuum (10^{-5} mbar). The involved amounts of the developed SILP systems and the corresponding supports were of the order of 50 mg, and degassing was performed at high vacuum (10^{-5} mbar) and temperatures of 433 and 453 K, respectively. It should be noted that outgassing temperatures were selected in relation to the results of DSC analysis and were set at least 100 K lower than the melting or decomposition temperatures. The maximum time allowed to reach equilibrium at each pressure step was 10 h, and the internal algorithm of the microbalance software detected equilibration within a period of 3−4 h.

Liquid nitrogen isotherms at 77 K were obtained, using the Autosorb-1 MP (Quantachrome) porosimeter. Before each measurement, the samples were degassed, under high vacuum 10^{-5} mbar for 24 h at the outgassing stations of the instrument. The outgassing temperatures were 433 K for the SILPs and 453 K for the supports and the silylated supports.

The X-ray diffraction (XRD) measurements were performed with a D8 Bruker system using Cu Kα radiation. The samples were in powdered form and were mounted on a glass slide. Measurements were carried out to both pristine and SILP samples.

Modulated DSC analysis was performed with a TA Instruments 2920 MDSC. The runs proceeded with a cooling down to −50 °C followed by an isothermal step of 10 min at this temperature and heating up to 330 °C with rates of 1.5 and 10 °C/min. The modulation parameters were set to 0.08 W/g for the amplitude and -2×10^{-4} W/g/°C for the slope. NMR spectra were obtained on a Bruker Avance/500 MHz spectrometer.

2.2. Synthetic Procedures. ***2.2.1. Chemicals.*** The following solvents and reagents were used as purchased without further drying or purification: toluene (puriss, Reag ACS, Aldrich), dichloromethane (GC 99.5%, Aldrich), chloroform (GC, Aldrich), methanol (P99.8, Aldrich), chlorobutane (P99%, Fluka), 1-methylimidazole (P99% redistilled, Aldrich), (3-chloropropyl)-triethoxysilane (95%, Aldrich), (3-chloropropyl)-trimethoxysilane (97%, Aldrich), sodium hexafluorophoshate (98%, Aldrich), and hexafluorophoric acid (60 wt % solution in water, Aldrich). Due to the high affinity of the [bmim][PF_6^-] to water, the gases used for the adsorption experiments were of high purity, CO_2 (99.998%, <3 vpm H_2O), CO (99.997%, <3 vpm H_2O).

2.2.2. Preparation of the Hybrid Material 1-(3-Silylpropyl)-3-methylimidazolium Hexafluorophosphate/Porous Support ([spmim][PF_6^-]/Vycor). The Vycor substrate was treated in the optimum rehydroxylation conditions as adequately defined and described in section 3.1.2. For the silylation procedure, reactivity parameters for optimum reaction conditions were studied. $CHCl_3$ as a solvent for a reaction time of 24 h at 0.4 M concentration (7.4 $mmol_{silylant}/g_{sample}$) was found to give the optimal surface coverage. The synthetic procedure of grafting the (3-chloropropyl)-trimethoxysilane on the surface was as follows: A solution of the silylating agent in the corresponding solvent was added to the solid support, and the mixture was stirred under reflux and N_2 atmosphere for 24 h. Then, the samples were washed by refluxing for 20 min sequentially in 40 mL of pentane and 40 mL of CH_3CN, and dried in a vacuum. The chloropropylated samples were treated with an excess of 1 methylimidazole and heated at 358 K under N_2 atmosphere for 48 h. Then, the samples were washed with toluene (2 × 15 mL at rt, 1 × 15 mL refluxed) and dried in a vacuum for 2 h.

To 0.74 g of hybrid [spmim][Cl^-] material a solution (0.05 M) of $NaPF_6$ (56 mg) dissolved in 7 mL of MeOH was added, and the mixture was rotated under N_2 atmosphere at room temperature for 90 h. The $AgNO_3$ test was positive from the first 24 h of reaction onset. The reaction mixture was filtered, and the sample was washed by reflux with MeOH (30 mL) for 15 min. After filtration, the sample was dried in a vacuum for ∼1 h.

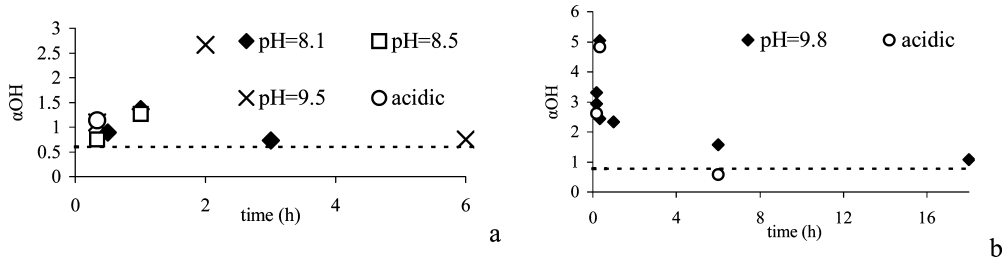

Figure 1. Effect of basic and acidic treatment period on the α_{OH} number (a) for Vycor and (b) for xerogel silica. Horizontal lines represent the α_{OH} number of the calcined samples.

TABLE 1: Hydroxyl Population Determined by Different Analytical Methods

	α_{OH} (μmol OH/m^2)								
	literature							this work	
	calcination at 823 K				rehydroxylated			calcination at 823 K	rehydroxylated
	NMR	TG	H_2O sorption	DRIFT	NMR	TG	H_2O sorption	H_2O desorption	
MCM-41	2−4,[31] 4−5[39]	2[39]	2.65[29]	1.5	5	4.4[27]		0.75	
xerogel silica[30]	2.9	3			8	8.5		0.77	2.6
Vycor			1.55[39]		3.8[39]			0.6	1.3

2.2.3. Preparation of the Hybrid Material 1-(3-Silylpropyl)-3-methylimidazolium Hexafluorophosphate/Porous Support ([spmim][PF$_6^-$]/MCM-41). A 200 mg portion of MCM-41 was dried at 423 K under a vacuum for 1 h. To the solid support, a solution of (3-chloropropyl)-trimethoxysilane (2.5 mL, 13.5 mmol) in $CHCl_3$ (10 mL) was added (67.5 $mmol_{silylant}/g_{sample}$) and the mixture was refluxed under stirring and N_2 atmosphere for 48 h. After filtration, the hybrid material was washed consequently by refluxing in pentane (30 mL), CH_3CN (30 mL), and diethyl ether (30 mL) followed by drying for 1 h at 343 K. Following, the chloropropylated hybrid material was reacted with 1-methylimidazole (5 mL) under N_2 atmosphere at 358 K and remained under rotation for 48 h. The reaction mixture was filtered and the hybrid material was refluxed with diethyl ether (30 mL) for 30 min and then filtered and dried at 343 K for 1 h.

To the synthesized [spmim][Cl$^-$] hybrid material a solution of $NaPF_6$ (68 mg, 0.4 mmol) in ethanol (6 mL) was added under N_2 atmosphere and the mixture remained under stirring for 5 days at room temperature. Reaction progress for the ion exchange step was monitored with the $AgNO_3$ test, which was positive from the first 24 h from reaction onset. The hybrid material was consequently filtered, washed by refluxing with methanol (30 mL) for 30 min, filtered, and dried in a vacuum for ∼1 h.

3. Results and Discussion

3.1. Surface Pretreatment. ***3.1.1. Methodology for Examining Surface Treatment Effects.*** The effect of basic and acidic treatment on the surface silanol group population for the several thermally annealed siliceous materials examined in this work is presented in Figure 1.

The α_{OH} values (μmol of OH/m^2) were calculated from the amount of water h_w (g/g) remaining adsorbed after 24 h of evacuation at 308 K and 10^{-4} mbar, assuming a one to one interaction/correspondence between the hydroxyl groups of the silanols and the water molecules. The following equation was involved for the calculation:

$$\alpha_{OH} = \frac{10^6 h_w}{M_w A_{BET}}$$

where M_w = 18 g/mol and A_{BET} (m^2/g) is the surface area of the material defined by LN_2 porosimetry. In Table 1, α_{OH} values are compared to those derived through alternative methods such as ^{29}Si cross-polarization magic-angle-spinning NMR (^{29}Si-CP-MAS NMR), isotopic exchange followed by ^{1}H NMR spectroscopy,[26] thermogravimetric analysis (TG) up to 1273 K,[27] diffuse-reflectance infrared Fourier-transform spectroscopy (DRIFT),[28] and water sorption BET analysis.[29]

Xerogel silica[30] and MCM-41,[31] dehydroxylated through thermal annealing at 823 K and rehydroxylated by refluxing in hydrochloric acid (18.5% w/w), as well as Vycor, dehydroxylated through thermal annealing at 823 K and rehydroxylated in H_2O_2 (30% w/w, 363 K) and sequential washings with deionized water, were adopted as reference materials to evaluate the validity of the water vapor desorption method, applied in this work. Comparing the surface hydroxyl numbers presented by different authors, one should consider that the results could depend on both the analytical techniques involved and the synthetic procedures of the corresponding mesoporous materials. However, as can be observed (Table 1), in all of the cases, our method underestimates the surface −OH population by a significant factor, on the order of 3. The rough assumption of a one to one interaction between the surface silanol groups and water molecules is also adopted in other studies using different techniques,[29] and thus, it cannot be considered as a reason for the −OH number underestimation. It is rather the hypothesis that all of the hydrogen-bonded water remains on the solid surface under the involved high vacuum conditions (10^{-4} mbar, 308 K) that generates this large discrepancy. From the several methods applied, DRIFT and ^{29}Si-CP-MAS NMR spectroscopy primarily provide qualitative information about the type of surface silanol groups and isolated terminal (≡SiOH), hydrogen-bonded terminal (SiOH···$^-$OSi), geminal (=Si(OH)$_2$), and associated geminal groups can be distinguished,[27] with relative populations depending on the heat treatment and rehydroxylation conditions of the material. The most important finding of these studies is that, from the different types of surface silanol groups, the isolated terminal (≡SiOH) exhibit the higher affinity toward water[27,32] and can be regarded as the most capable of retaining hydrogen-bonded H_2O molecules under high vacuum. On the basis of the latter concept, we suggest that our method provides an estimate of the, more reactive, isolated terminal silanols alone,

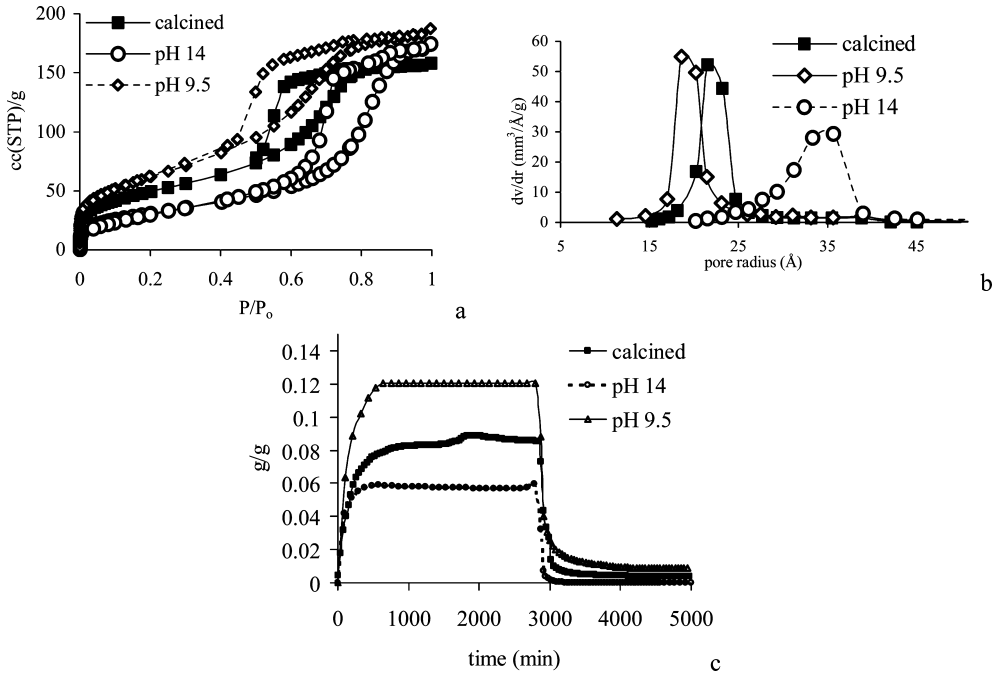

Figure 2. (a) LN_2 adsorption desoprtion curves, (b) corresponding PSD distributions, and (c) water adsorption desorption cycle.

as these are the first silanol groups to be anchored with the silylating agents.[33] Although thermogravimetric analysis up to 1273 K is the more direct and accurate method for the calculation of the surface hydroxyl number, thermal stability limitations prevent the determination of the extent of organic grafting through this approach. Thus, we propose the water desorption method as a simple procedure, instead of the more complicated isotopic exchange ^{1}H NMR and DRIFT spectroscopies, in order to compare materials treated under different conditions and investigate the degree of their hydroxylation and silanization.

3.1.2. Effects of Rehydroxylation Conditions. Figure 1a shows that in the case of Vycor and under mild basic hydrolysis conditions (pH 8.1−9.5) at room temperature, the period of treatment rather than the pH is the most important parameter and the α_{OH} value presented a maximum after about 2 h of sonication in a NH_3 solution of pH 9.5, whereas, for treatment periods well in excess of 2 h, extended leaching of the surface led to a moderate population of the hydroxyl groups. Moreover, acidic hydrolysis with a solution of H_2SO_4/H_2O_2, 4/1, for 20 min, presented similar to the NH_3 solution (pH 9.5) efficiency in regenerating surface silanol groups. In the case of xerogel silica and under stronger basic conditions (pH 9.8), a treatment period of under 0.5 h suffices for the full rehydroxylation of the surface (Figure 1b), whereas 333 K was the optimum treatment temperature. Acidic treatment (H_2SO_4/H_2O_2, 4/1) at 333 K, identical to the basic treatment periods, was found less efficient in regard to the capacity to regenerate surface hydroxyls (Figure 1b).

The ability of the material to retain its pore structure unaffected under the involved basic hydrolysis conditions was investigated with LN_2 porosimetry and the water adsorption/desorption cycles. As it can be observed from the N_2 (77 K) isotherms (Figure 2a), Vycor treated at the optimum hydroxylation conditions (pH 9.5, 2 h) exhibits higher surface area and slightly smaller pore size (inset) compared to the calcined sample.

This is because the introduced surface silanols act as adsorption sites during the monolayer formation and enhance the surface roughness (fractality), whereas during the subsequent multilayer adsorption the nitrogen t-layer starts to form at a distance from the pore walls, determined by the space occupied by the silanol groups. The higher pore volume (by a factor of 1.15) results from the leaching of amorphous siliceous matter that had remained on the pore mouths during the fabrication of porous glass and obstructed access to a small portion of the porous network.

An interesting issue arises upon comparison of the pore volume enhancement calculated from LN_2 adsorption and H_2O adsorption (up to a P/P_o ratio of 0.8), respectively. In the case of water and nitrogen, the enhancement factor was 1.4 and 1.15, respectively. This can be explained in terms of a previous study of our group[34] where it was shown that silicate entities (silanols) emanating from the surface of dry Vycor pores are bent and attached to the pore walls through the action of adsorbed water at small relative pressures, corresponding to the area of the monolayer completion. Thus, apart from the already described leaching effect, the pore volume available for capillary condensation is enhanced by a larger factor in the case of water. On the other hand, the extended leaching of a Vycor sample treated at pH 14 for 15 min can lead to elimination of certain fine features of the silica framework such as thin necks; such a process will lead to pore merging and surface area reduction. Indeed, as shown in Figure 2a (inset), the pore size distribution shifts to larger pore size and the surface area is drastically reduced. The Kelvin equation requirements for capillary condensation were not fulfilled for a major portion of the pore structure in the case of water, due to the larger pore size, and this explains the lower amount of adsorbed water at $P/P_o = 0.8$ ($r_k = 2.23$ nm) (Figure 2b).

3.2. Silanization. In Table 2, we summarize the results of nitrogen porosimetry and elemental analysis (TC) of the silanized Vycor samples (V1−V5) in relation to the grafting extent G_g and G_s calculated from the water desorption method (Figure 3) through the following equations:

$$G_g\,\% = 100\frac{hg_{vyc} - hg_{sil}}{hg_{vyc}} \qquad G_s\,\% = 100\frac{hs_{vyc} - hs_{sil}}{hs_{vyc}}$$

where hg_{vyc} and hg_{sil} are the mass of water remaining adsorbed per mass of the Vycor sample and the silanized sample, respectively, and hs_{vyc} and hs_{sil} is the mass of water remaining adsorbed per the specific surface area of the materials. The silanization reaction parameters are also included in this table.

To ensure sufficient surface coverage, the involved concentration (mmol/g) of the 3-(chloropropyl)trimethoxysilane per mass of the solid was well in excess of the surface hydroxyl concentration ($1000hg_{vyc}/18$), which was 0.24 mmol/g for the H_2O_2 (30%) treated and 0.47 mmol/g for the fully rehydroxylated Vycor at pH 9.5 for 2 h.

The accordance between the carbon content derived from elemental analysis and this calculated from the grafting extent further supports the statement that the water desorption method produces quite reliable results when the purpose is the quantitative evaluation of the silanization process. A first issue to be discussed is the effect of solid surface pretreatment on the silane grafting extent. A heat treatment at 453 K was selected as the most appropriate to remove surface adsorbed water without in parallel affecting the surface silanol groups and especially the geminal that may suffer condensation reactions at temperatures not far above 473. Independently of the reaction solvent, the solid pretreatment significantly enhanced the grafting extent by a factor of 1.2−1.3.

Adsorbed water on the surface of the untreated sample hydrolyses the unreacted alkoxy groups of the already grafted silanes. This creates hydroxyl groups in addition to the existing surface hydroxyls, which were hindered from reacting with the oncoming silanes. Therefore, the silanization process further evolves with two possible mechanisms (Figure 4): (A) additional surface coverage through the reaction of oncoming silane molecules with the unhindered (due to the removal of the alkoxy groups) surface hydroxyls and polymerization of the adjacent grafted silanes; (B) the already grafted silane molecules are polymerized with the oncoming silanes leading to the formation of bulky organosilane entities and leaving in parallel a portion of the surface hydroxyls unaffected.

The lower grafting extent values G_g observed for the untreated solids confirm the occurrence of mechanism B. In the case of the more hygroscopic toluene, the presence of residual water

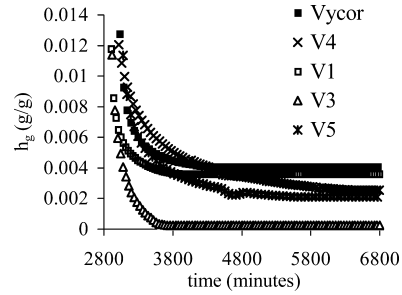

Figure 3. Water desorption of the Vycor and the silanized samples.

in the solvent facilitates the formation of even bulkier organosilane entities, generated by silane polymerization before anchoring with the solid surface hydroxyl groups (Figure 4C). Steric effects prohibit polymerized silanes to be anchored to vicinal hydroxyls, and this explains the significantly lower grafting extent values when compared to those obtained when chloroform was used as a silanization solvent. The lower pore volume and BET surface areas extracted from the LN_2 isotherms of the silanized toluene samples (Table 2) also confirm the aforementioned mechanism. Moreover, the moderate alteration of the BJH derived pore size distribution as compared to Vycor (Table 2) leads to the conclusion that the formed bulky entities are not continuous but randomly distributed on the pore surface. Further issues concerning the fractal characteristics of the Vycor surface after silanization have been extensively investigated in a previous study of our group via SAXS analysis.[23] In brief, it had been shown that moderate grafting extent like in the case of dichloromethane (sample V1) did not induced any alteration of the initial fractal dimension of the dry sample but rather an insignificant increase. This is further verified by the slightly higher surface area as compared to that of the dry Vycor (Table 2) and can be explained by the fact that the protruding silane molecules induce more sites for N_2 adsorption than they occupy. In all of the other cases, the surface fractal dimension D_s was reduced due to the low or high degree of silane polymerization. The derived fractal dimensions D_s varied on the order (dichloromethane/untreated solid) > Vycor > (chloroform/untreated solid) > (toluene/treated solid) > (toluene/untreated solid), which is consistent with the above-described grafting and polymerization routes of the silanes.

The polarity of the solvent is a very important parameter for the silanization reaction. For the type II SN2 mechanism

TABLE 2: Effect of Silanization Conditions on the Grafting Extent

		Vycor					
		V1	V2	V3	V4	V5	
solvent		CH_2Cl_2	$CHCl_3$	$CHCl_3$	toluene	toluene	
polarity index		3.1	4.1	4.1	2.4	2.4	
reflux temperature (K)		313	334	334	383	383	
silylant concentration (M)		0.05	0.44	0.37	0.46	0.44	
$mmol_{silylant}/g_{sample}$		1.8	7.3	7.4	5.5	5.5	
reaction time (h)		24	24	24	24	24	
sample pretreatment[a]		−	−	+	−	+	
BET surface area (S_{BET})	m^2/g	200	202	179	165	142	142
total pore volume (TPV)	mL/g	0.24	0.25	0.22	0.2	0.17	0.19
mean pore size, BJH method	nm	2.00	1.85	1.85	1.85	1.75	1.85
hg_i	g/g	4.3×10^{-3}	3.6×10^{-3}	8.6×10^{-4}	2.5×10^{-4}	2.6×10^{-3}	2.1×10^{-3}
hs_i	g/m^2	2.2×10^{-5}	1.8×10^{-5}	4.8×10^{-6}	1.5×10^{-6}	1.8×10^{-5}	1.5×10^{-5}
grafting extent (G_g/G_s)	%		16/17	80/78	94/93	40/15	51/31
carbon content[b]	% C		0.23	1.15	1.35	0.57	0.73
carbon content experiment	% C		0.31	1.08	−	−	0.8

[a] At 453 K and high vacuum. [b] Calculated out of the grafting extent.

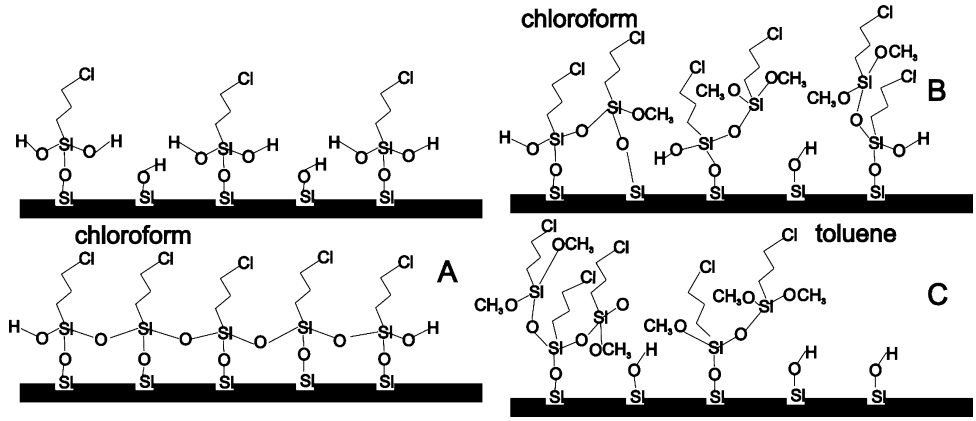

Figure 4. The proposed configurations of surface silanization: (A, B) silanization in chloroform on a non thermally treated surface; (C) silanization in toluene.

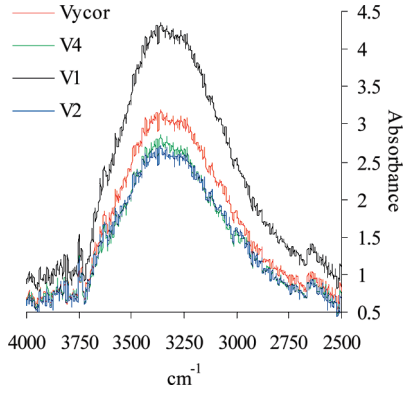

Figure 5. FTIR spectra of Vycor and the silanized Vycor samples.

(expected to be involved in the reaction under consideration), where the reactants are neutral, reactivity is expected to be enhanced by polar solvents. As it can be seen from Table 2, the grafting extent correlates well with the polarity of toluene and chloroform. However, the presence of trace water in toluene or on the solid surface, that induced quite different silanization mechanisms, does not permit for the extraction of reliable conclusions about the polarity effect. Also, the solvent reflux temperature favors the direction of a faster diffusion of the reacting silanes into the nanoscale pores of the involved materials. In this work, the reaction time applied for all of the samples (24 h) was extended enough and thus it did not allow for an investigation of diffusion limitations.

Furthermore, in Figure 5, we present results of FTIR analysis for the Vycor and some of the silanized samples. The well-resolved vibration band at 3740 cm^{-1} belongs to the isolated terminal silanol groups. Additionally, a broad absorption is observed in the region 3500−3200 cm^{-1}, due to the H-bonded geminal and associated terminal silanol groups. Remarkably, surface water that had not been removed during the treatment (vacuum for 3 h at room temperature) of the samples just before the FTIR analysis had also a significant contribution in the energy range 3500−3200 cm^{-1}. Interesting enough is that the intensity of this broad band correlates positively with the S_{BET} of the examined samples and negatively with the grafting extent of the silanized samples (Table 2). According to the above discussions for the moderately silanized sample V1, the unreacted alkoxy groups of the grafted silane molecules can be further hydrolyzed, creating excess hydroxyl groups in addition to the remaining free surface hydroxyls. Polymerization reaction between the grafted silanes is prohibited due to the high distance among them and this explains the higher intensity of the 3500−3200 cm^{-1} absorption band compared to this of Vycor. Normally, for the other two extensively silanized samples (V2, V4), the absorption band was of lower intensity than this of Vycor due to the enhanced anchoring on the surface hydroxyls and the polymerization reactions that consume the unreacted alkoxy groups. However, the band intensity ratio was not quite relevant with the grafting extent ratio between these two samples and this can be again attributed to the hydrolysis of unreacted methoxy groups that seems to happen in a higher extent for sample V2.

3.3. Absorption Results. ***3.3.1. Absorption in the Bulk Ionic Liquid Phase.*** In Figure 6, we present the results of CO_2 and CO absorption at different temperatures in the three bulk ionic liquid phases examined in this work.

Gas absorption properties were for the first time studied at a temperature of 273 K, which is about 6 K below the melting point of the bulk ionic liquid [bmim][PF_6^-]. However, after considering several studies describing the difficulty to obtain stable [bmim][PF_6^-] crystals by cooling, as solidification often results in glass formation,[35,36] we cannot claim that at this temperature the ionic liquid was in its solid state.

As it can be observed, independently of the IL physical state, the carbon dioxide follows the exothermic character of solvation in both the commercial [bmim][PF_6^-] and the synthesized [spmim][PF_6^-]. The Henry constants ($\bar{H}$, bar/mol fraction) correlated positively with temperature. The $\bar{H}$ values of 31.9, 40.3, and 63 bar/(mol fraction) calculated for the commercial ionic liquid at 273, 288, and 308 K, respectively, were in good accordance with those often encountered in the literature.[14] The $\bar{H}$ value of the synthesized [bmim][PF_6^-] (33.8 bar/mol fraction) at 273 K deviated no more than 6% from that of the commercial one, and this signifies the purity of the synthesized ionic liquid phase. It should be noted that the absorption results presented in Figure 6a were normalized over the entire mass of the bulk ionic liquid absorbents. However, in the case of the synthesized alkoxysilyl-IL [spmim][PF_6^-] and in order to derive reliable conclusions, absorption results should be normalized per the net mass of the 1-propyl-3-methylimidazolium-hexafluorophosphate ([pmim][PF_6^-]) in the alkoxysilyl-IL molecule, since the silyl part is not expected to have any remarkable contribution on the CO_2 absorption capacity. By applying a (silyl/[pmim][PF_6^-]) mass fraction of 0.45 as calculated from the stoichiometry of the molecule and with the assumption that hydrolysis of the silyl part of the silylated IL was completely avoided under the involved conditions of inert atmosphere and high vacuum, we derived an $\bar{H}$ value of 39.2 bar/(mol fraction)

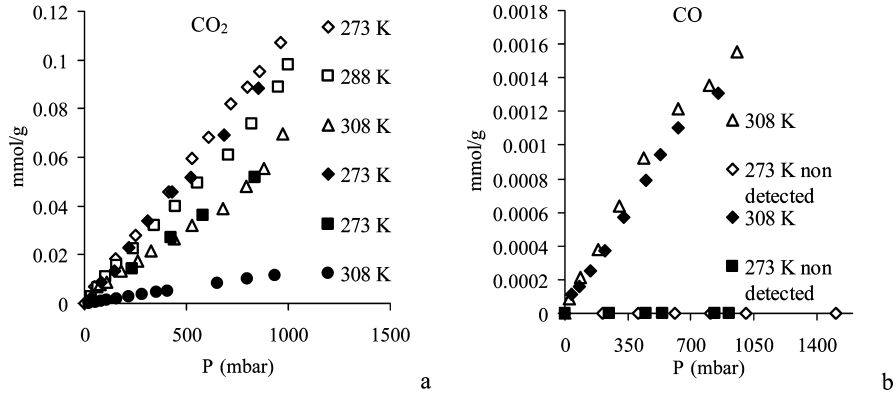

Figure 6. (a) Open symbols: commercial [bmim][PF_6^-], filled rhombs: synthesized [bmim][PF_6^-], filled rectangles-filled cycles: synthesized [spmim][PF_6^-]. (b) Open symbols: commercial [bmim][PF_6^-], filled rhombs: synthesized [bmim][PF_6^-], filled rectangles: synthesized [spmim][PF_6^-].

at 273 K for the synthesized alkoxysilyl-IL. There are two possible reasons for the lower absorption capacity of the silylated-IL.

The first has to do with the number of carbon atoms in the alkyl chain of the imidazolium ring that is 3 for the [spmim][PF_6^-] and 4 for the bulk ionic liquid [bmim][PF_6^-]. Although several studies revealed that only the anionic part of the IL significantly affects the CO_2 solubility,[37] changes in the imidazolium cation involving alkyl groups were also proved to have a relatively moderate influence on the gas solubility properties. In fact, the longer alkyl chains usually resulted in a slightly better CO_2 absorption capacity in the ionic liquid, but there are not sufficient explanations about this issue.[38,39] In our case, the effect of the carbon atom number seems to be more enhanced as the Henry constant ratio for a difference of one carbon number in the alkyl chain was 0.87 compared to ratios of 0.94 often found in the literature[38] for differences of 2 up to 4 carbon atoms. On the basis of this fact, we can claim that the lower CO_2 solubility value mainly arises as an effect of the silyl group, attached to the alkyl chain of the imidazolium ring. Recent MD simulations indicated that CO_2 organizes strongly about the [PF_6^-] anion in a "tangentlike" configuration that maximizes favorable interactions[37] which enhance its solubility. The presence of the silyl group may lead to a modest loss of organization of the anion and the CO_2 about the cation as also had occurred in other studied cases where the acidic hydrogen on the C2 carbon of the [bmim] cation was replaced with a methyl group.[37]

Concerning the CO solubility (Figure 6b), this was detectable just for the commercial and the synthesized [bmim][PF_6^-] at 308 K. The calculated $\bar{H}$ values of 2158 and 2202 bar/(mol fraction), respectively, were in good accordance with those found in the work of Kumelan et al.,[12] and deviated positively by approximately 100% from those found in the studies of Jacquemin et al.[13] Interesting enough is that, for the ionic liquid [bmim][PF_6^-] at 273 K, the CO absorption was undetectable, producing negative erroneous values for the amount absorbed. Thus, the CO_2/CO selectivity rises from the value of 40 at 308 K to infinite at 273 K. Moreover, in both of the aforementioned studies, the calculated Henry constant $\bar{H}$ values for CO practically did not depend on temperature and more specific in the work of Kumelan et al. they even had a negative correlation, as also holds in our case, showing that the amount absorbed increases with temperature. This different solvation behavior of the carbon monoxide has been already emphasized in several studies by the calculated zero enthalpy of solvation compared to the negative values calculated for the carbon dioxide and the other investigated gases.[13] This indicates that the crossed gas−ionic liquid molecular interactions are of different nature in CO and in CO_2. As will be shown in the following sections, independently of the temperature, the examined ionic liquid under extreme confinement into the small pores of the MCM-41 supports was in its solid state. This implies enhanced IL stability and infinite CO_2/CO selectivity even at elevated temperatures, rendering the developed SILP systems potential candidates for PSA applications.

3.3.2. Adsorption on the Pristine Supports and Absorption in the SILP Systems. In Figure 7, we present the obtained CO, CO_2, and LN_2 isotherms for the small pore size (2.3 nm) MCM-41 and the relevant supported ionic liquid phase (SILP) system.

As is clear from the nitrogen porosimetry results, the pores of the MCM-41, having a mean size of 2.3 nm, were totally occupied by the developed silyl/ionic liquid phase. The upward step of the LN_2 isotherm at a relative pressure close to unity, observed for both the SILP and the MCM-41, is attributed to nitrogen condensation in the interparticle void volume of the solid support. On the basis of the results of LN_2 porosimetry, it can be stated that the further described CO_2 and CO absorption capacity of the developed SILP is only related to the inherent solvation properties of the [spmim][PF_6^-] phase that fully occupied the pores of MCM-41. This is the reason we adopted the term absorption for the SILP systems. As an exception to this statement, we note that the higher CO_2 amount absorbed in the SILP at the low-pressure region and the relevant curvature in the absorption curve (Figure 7b), compared to that in the bulk [bmim][PF_6^-], arise as a result of the contribution of the external surface area of the support particles. On the other hand, the CO_2 absorption capacity at higher pressures, above 5 bar, appears artificially lower due to the normalization over the entire mass of the hybrid SILP material. The entire mass of the hybrid material comprises the mass fraction of the MCM-41 support that has negligible contribution to the CO_2 uptake at high pressures. An interesting feature is that the CO_2 absorption in the SILP system (inset of Figure 7b) did not follow the exothermic character observed for the commercial ionic liquid [bmim][PF_6^-] (section 3.3.1). Indeed, the isotherms obtained at two quite different temperatures seem to come in convergence and their slight difference could lie within the accuracy limits of the microbalance setup, as suggested by the error bars. However, we can still note the significant contribution of the support external surface at low CO_2 pressures and the low temperature (273 K) and the higher CO_2 solubility at the higher temperature (308 K) for pressures above 5 bar. This inversion of the CO_2 solubility dependence on temperature, observed for

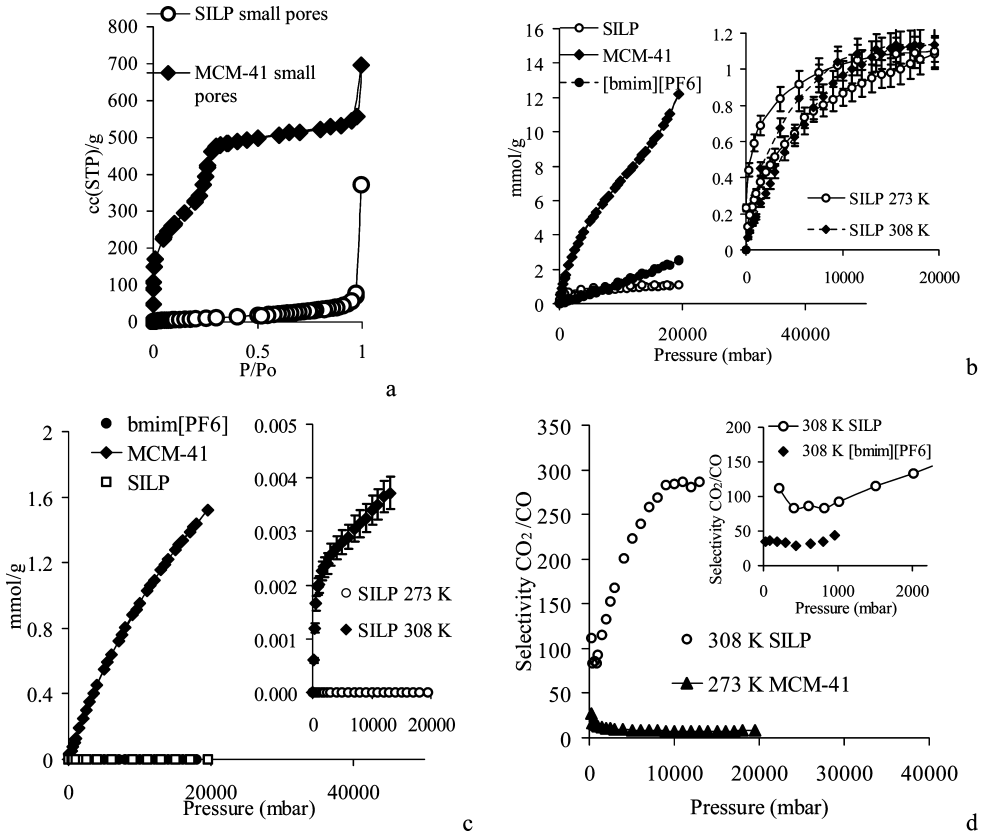

Figure 7. (a) LN_2 (77 K) isotherms. (b) CO_2 isotherms at 273 K. Inset: CO_2 absorption in the SILP (MCM41-2.3 nm) at different temperatures. (c) CO isotherms at 273 K. Inset: CO absorption in the SILP at different temperatures. (d) CO_2/CO selectivity vs pressure.

the SILP system, was a first indication that the developed ionic liquid [spmim][PF_6^-] phase under extreme confinement was in a different state other than the bulk liquid state. A possible existence of crystallinity in the developed ionic liquid may be responsible for the higher amount of CO_2 dissolved at the higher temperature as besides expected from the dissolution dependence on temperature for solids. Supporting discussions on that, in relation with the results of XRD and DSC analysis, are found in section 3.4. Finally, the CO_2/CO selectivity at 273 K for the SILP and the ionic liquid [bmim][PF_6^-] was infinite as a result of the zero CO solvation and for this reason it is not included in the selectivity plots (Figure 7d).

At 308 K and pressures up to 1 bar, the SILP, CO_2/CO selectivity values (100) were about double those of the bulk ionic liquid [bmim][PF_6^-], and this again indicates different solvation properties related to the different physical state of the developed [spmim][PF_6^-] phase under extreme confinement into the pores.

As it can be devised when examining the nitrogen porosimetry curve (Figure 8a) of the second SILP system, which was developed on the larger pores MCM-41 support (3.3 nm), the blockage of the void space was significant but not complete. The upward step of the LN_2 isotherm at relative pressures close to unity is again attributed to phenomena of capillary condensation in the interparticle void volume of the solid.

There are two observations that could further support the above stated incomplete occupation of the pore space in the larger pores of the MCM-41. In contrast to the SILP developed in the support with the smaller pores, the CO_2 adsorption followed the usual exothermic trend (inset of Figure 8b), emphasizing the fact that, after the silane grafting and sequential treatment with methyl-imidazolium and anion exchange with PF_6^-, there must still exist a void pore space that significantly contributes to the CO_2 uptake and defines the characteristics of the adsorption isotherm. On the other hand, the exothermic character of the CO_2 adsorption could also be attributed to the probability that the developed into the larger pores [spmim][PF_6^-] phase do not crystallize and retains the absorption characteristics of the bulk liquid (IL). However, as will be shown in the following paragraph, this statement does not hold.

What arises as a stronger evidence for the persistence of an open pore space is that the CO adsorption was detectable even at 273 K, something that was observed neither for the bulk IL nor for the SILP developed on the 2.3 nm support. Interesting enough is also that the SILP developed in the 3.3 nm MCM-41 support exhibited a much lower CO_2 adsorption capacity than the one developed in the small pores support. This contradicts the fact that the MCM-41 with the larger pores processes a more open porosity and consequently a larger pore volume and should have accommodated higher amounts of the developed [spmim][PF_6^-] phase. However, since the deposition of the IL phase starts from a surface reaction and proceeds to the bulk of the pore, it is wiser to interpret ionic liquid loadings in relation to the initial specific surface area of the supports. Indeed, the BET surface area is 1205 and 1120 m^2/g for the 2.3 and 3.3 nm MCM-41, respectively, and this justifies a higher IL loading into the smaller pores support. The CO adsorption capacity increases with temperature (Figure 8c), as was the case for the bulk [bmim][PF_6^-]. Interesting enough is the extended hysteresis of the CO even at very low pressures that can be attributed to diffusion limitation phenomena during absorption. This means that, although the allowed experimental time for equilibration was 10 h, the absorption isotherm points were still obtained in the transient state of each pressure increment due to the extremely slow rate of diffusion. In what concerns the performance of the developed SILP, the CO_2/CO selectivity had the

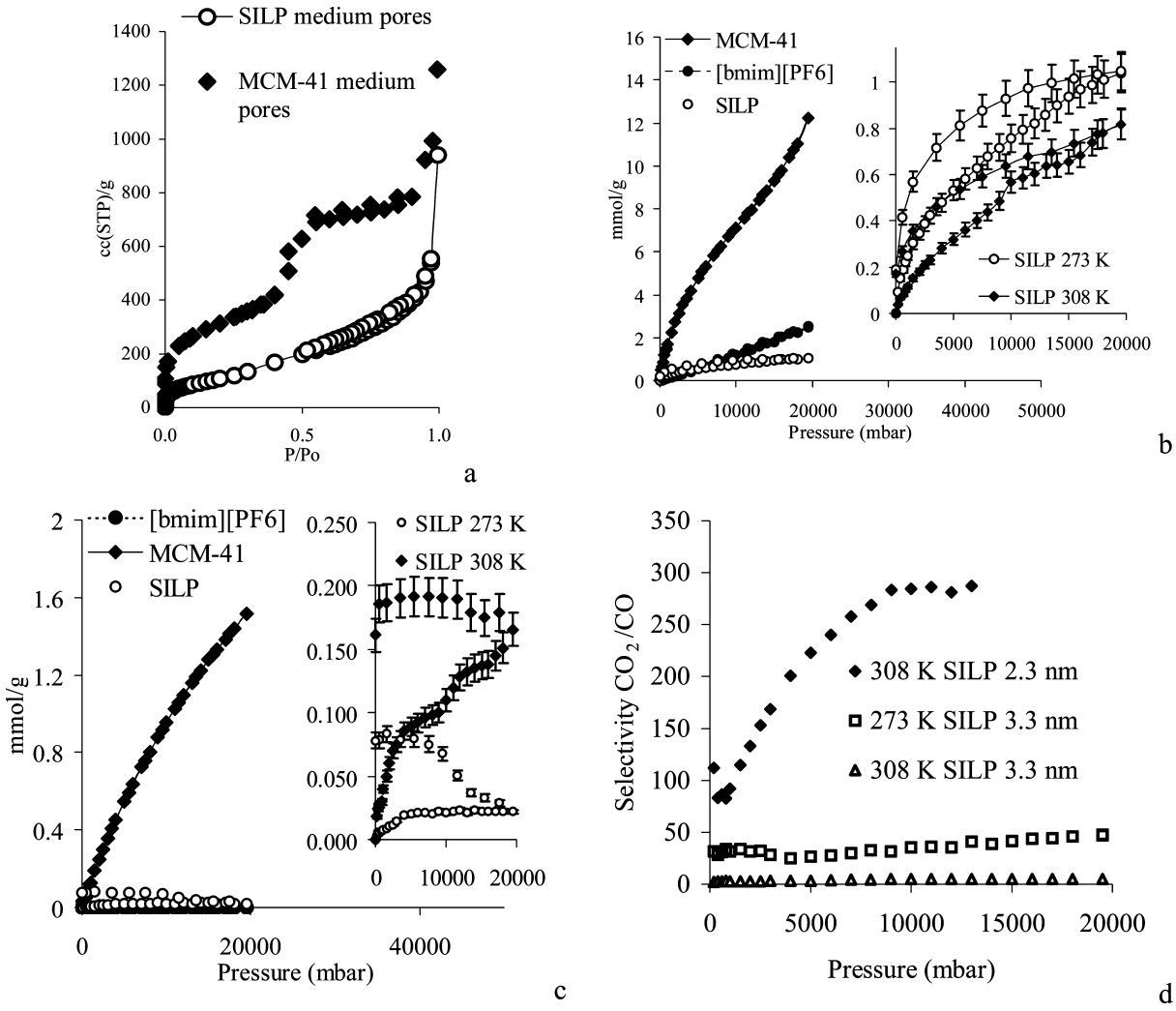

Figure 8. (a) LN_2 (77 K) isotherms. (b) CO_2 isotherms at 273 K. Inset: CO_2 absorption in the SILP (MCM41-3.3 nm) at different temperatures. (c) CO isotherms at 273 K. Inset: CO absorption in the SILP at different temperatures. (d) CO_2/CO selectivity vs pressure.

value 50 at 273 K (Figure 8d), which is by far superior to the performance of the pristine 3.3 nm MCM-41 support, which gave a CO_2/CO selectivity of 8. However, the incomplete coverage of the void volume of the pores considerably suppressed the separation performance that was about 5 at 308 K, when compared to the value of 280 obtained for the SILP developed on the small pore size support (Figure 8d).

In the case of Vycor (Figure 9), the extent of pore blockage was negligible and no enhancement of the CO_2/CO separation capacity of the SILP compared to the pristine support was observed.

Interesting enough is that there was not any alteration of the pore size of the SILP system (inset of Figure 9a). This indicates that regardless of the surface activation procedure, which resulted in a α_{OH} number of 2.6 μmol/m^2 or 1.6 OH/nm^2 (Figure 1a), the distance between the surface hydroxyls remained rather high to permit for the formation of a continuous [spmim][PF_6^-] layer. Additionally, the extremely tortuous structure of the porous glass compared to the MCM-41 support may considerably affect the transport of the solvent and reactants through the capillary channels, especially due to solvent evaporation, resulting in a poor [spmim][PF_6^-] loading.

The CO_2 and CO isotherms followed the exothermic character of adsorption as a result of the significant contribution of the Vycor open pores, whereas the CO_2/CO selectivity of the SILP system at 273 K was better than this of the Vycor support (Figure 9d) only at pressures up to 500 mbar. This is because in the very low pressure region the effect of the CO_2 solvation in the [spmim][PF_6^-] phase becomes more evident due to the small amounts of CO_2 and CO that are stacked on the open pore surface forming the adsorbed monolayer.

3.4. DSC and XRD Results. In Figure 10, the results of modulated DSC analysis for the SILP developed on the 2.3 nm MCM-41 support are presented in comparison with those for the pristine MCM-41 support.

The reversing component of the SILP comprises an endotherm in the area of 260 °C that was larger in the case of faster heating (10 °C/min), as expected for a heating rate dependent reversing transition. This endotherm is attributed to melting of the developed [spmim][PF_6^-], which was already crystallized at room temperature (see XRD, Figure 12b) under the extreme confinement into the 2.3 nm pores. The second endotherm at 320 °C, appearing only in the nonreversing component of the MDSC, was the result of the thermal decomposition of [spmim][PF_6^-] (Figure 10b). As can be observed in Figure 10b, the melting endotherm comprises also a nonreversing component. This change in behavior can be explained as follows. During the early stages of melting, the presence of many crystallites facilitates melting and recrystallization as heating modulation occurs. Eventually, however, all of the crystallites (sites for recrystallization) have melted and recrystallization cannot occur. At that point, melting becomes nonreversing. The

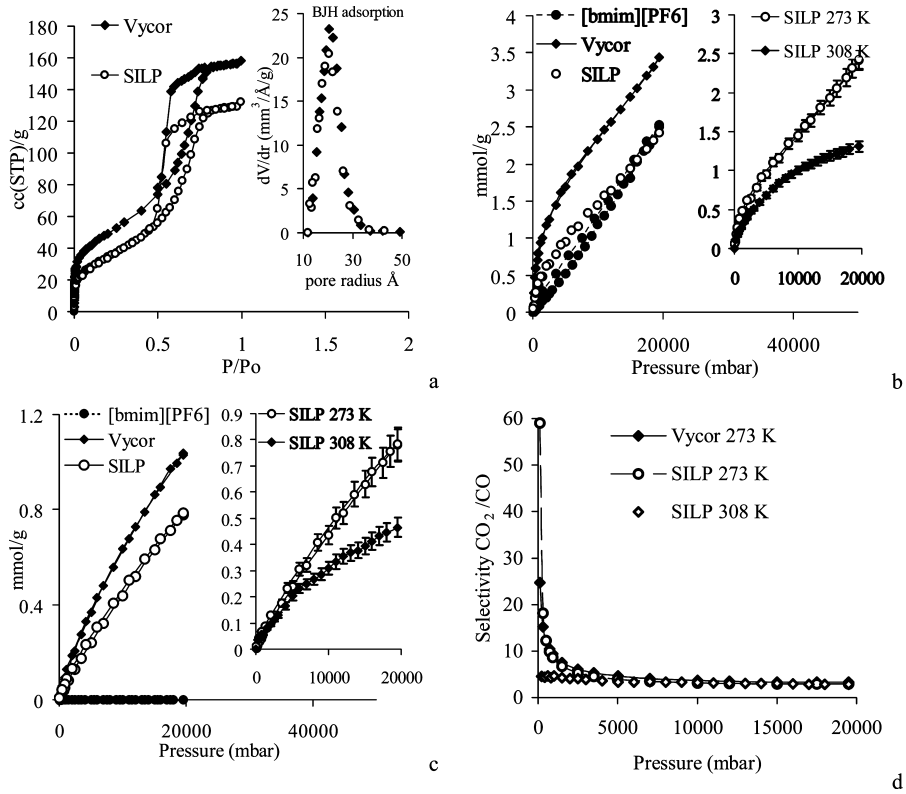

Figure 9. (a) LN_2 (77 K) isotherms. Inset: BJH pore size distribution of the Vycor and SILP from the adsorption branch. (b) CO_2 isotherms at 273 K. Inset: CO_2 absorption in the SILP (Vycor) at different temperatures. (c) CO isotherms at 273 K. Inset: CO absorption in the SILP at different temperatures. (d) CO_2/CO selectivity vs pressure.

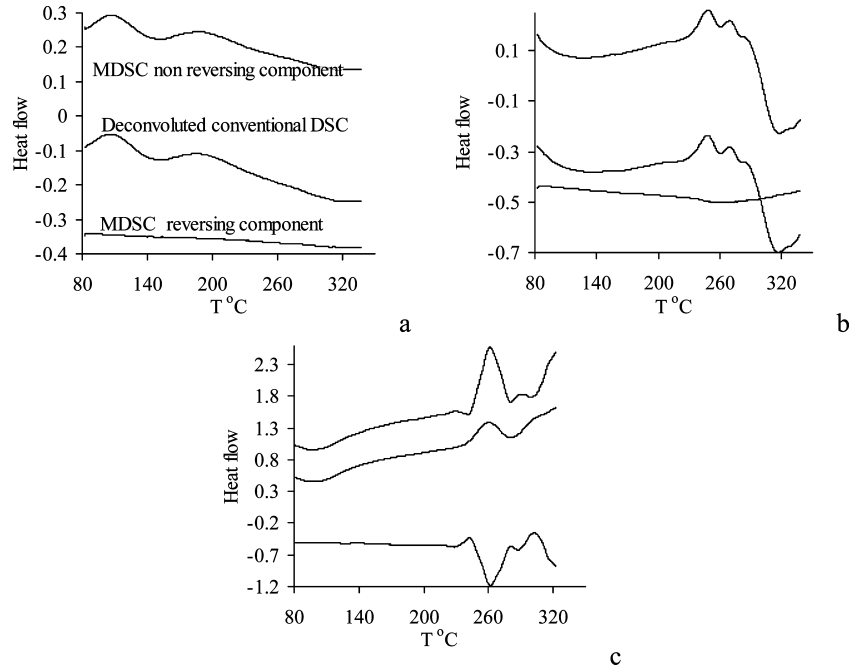

Figure 10. (a) MDSC analysis of pristine MCM-41, 2.3 nm, heating rate 1.5 °C/min. (b) MDSC analysis of the SILP, heating rate 1.5 °C/min. (c) MDSC analysis of the SILP, heating rate 10 °C/min. The lines from top to bottom of the plots correspond to nonreversing, conventional, and reversing components.

relative amount of reversing and nonreversing melting behavior depends primarily on the modulation frequency, but further investigations were not performed on this issue. Finally, the high heating rate did not allow well-resolved melting and decomposition endotherms to be obtained (Figure 10c).

The development of the [spmim][PF_6^-] phase into the Vycor pores is verified by the decomposition endotherm at 320 °C (Figure 11b), in good accordance with the endotherm observed in the case of the MCM-41, 2.3 nm support.

The higher heat rate (Figure 11b) did not induce any alteration on the intensity of the nonreversing, temperature dependent decomposition event, except from a slight shift of its occurrence temperature at 300 °C. No signs of [spmim][PF_6^-] crystallization were observed, as also concluded from the XRD analysis of the sample.

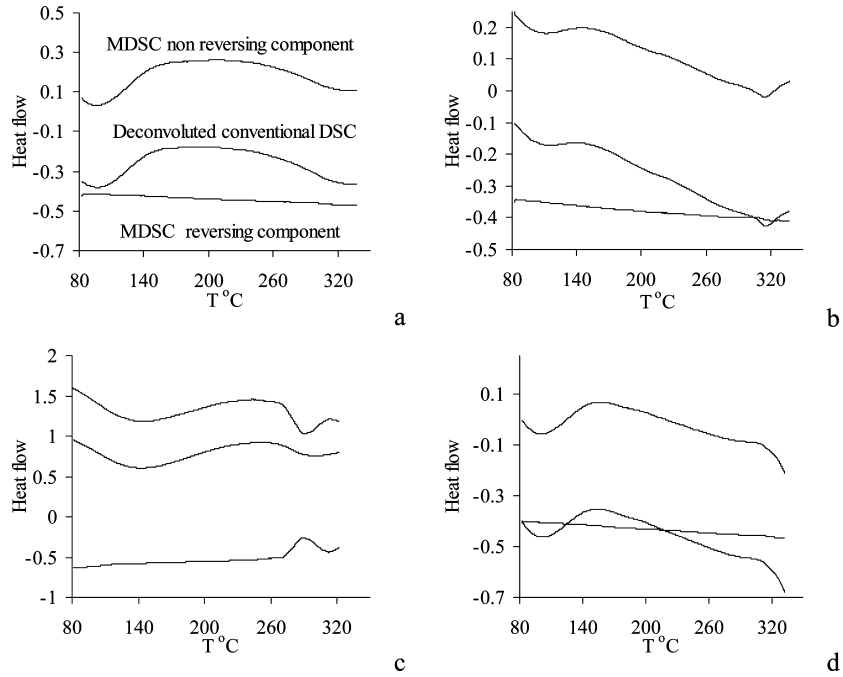

Figure 11. (a) MDSC analysis of pristine Vycor, 4 nm, heating rate 1.5 °C/min. (b) MDSC analysis of the SILP, heating rate 1.5 °C/min. (c) MDSC analysis of the SILP, heating rate 10 °C/min. (d) MDSC analysis of silanized Vycor, heating rate 1.5 °C/min.

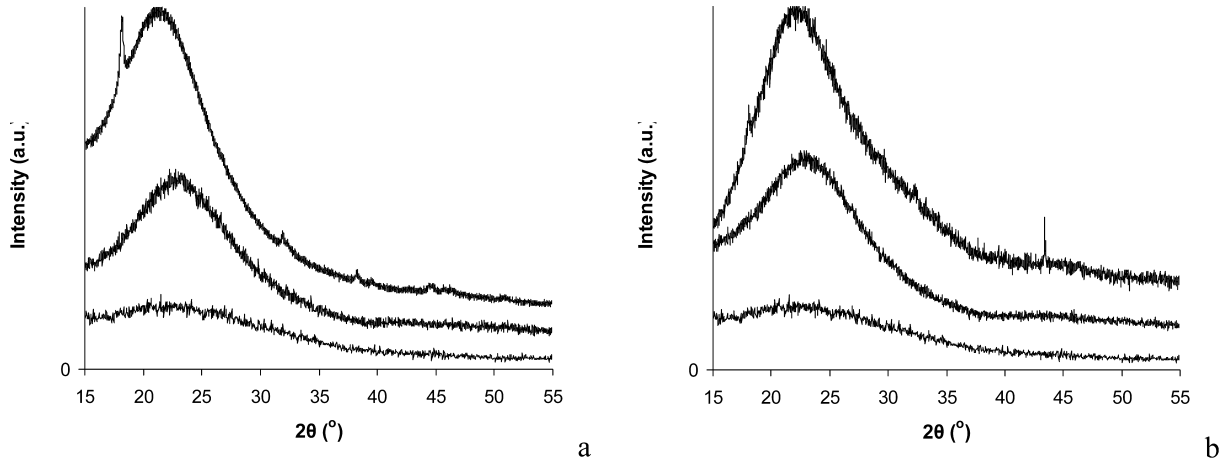

Figure 12. (a) X-ray diffraction spectra (from bottom to top) of glass, pristine MCM-41, 3.3 nm, and the correspondent SILP system. (b) X-ray diffraction spectra (from bottom to top) of glass, pristine MCM-41, 2.3 nm, and the correspondent SILP system.

Finally, in Figure 11d, we present the thermogram of the silanized sample. The decomposition of the grafted silane molecules starts at temperatures well above 320 °C, and on this concept, we can claim that the presence of silane does not degrade the thermal stability of the developed [spmim][PF_6^-]. On the contrary, we can claim that the grafted [spmim][PF_6^-] ionic liquid has a better thermal stability than the bulk [bmim][PF_6^-] (290 °C).

Figure 12a illustrates the diffraction spectra of both pristine (3.3 nm) MCM-41 and the correspondent SILP sample developed on the MCM-41 support. The background pattern (glass slide) is presented too. Compared with the pristine sample, the SILP sample shows diffraction peaks appearing at $2\theta = 18.2$, 31.9, 38.2, 39.4, 44.5, 46.2, and 50.9°. The result strongly suggests the formation of [spmim][PF_6^-] crystals within the pores of the nanoporous material. This transition might be attributed to the IL confinement within the pores of the nanostructured materials. Chen et al.,[24] based on DSC and XRD analysis, have also reported the transition of IL [bmim][PF_6^-] from liquid to high-melting-point crystal when confined in multiwalled carbon nanotubes. In addition, some of their reported peaks (first, fourth, sixth, and seventh) are comparable to ours, implying that the solid phase formed inside the carbon nanotubes has similarities with the one formed within the pores of MCM-41. However, the IL when confined inside nanotubes[24] and pores at room temperature differs structurally from the low-temperature crystal reported by Choudhury et al.[37] As in the case of the IL encapsulated inside the nanotubes, a detailed investigation of the IL crystal structure within the pores of the MCM-41 support is difficult and out of the scope of the present study.

Figure 12b presents the diffraction patterns of both pristine (2.3 nm) MCM-41 and the SILP sample. In this case, only the $2\theta = 18.1$ and 32.3° peaks might be attributed to the silylated IL crystallization due to its confinement in the pores, suggesting a short-range order. A possible explanation for the moderate peak intensities could be the smaller amount of the IL required for development on the support material, due to its smaller pore size. The sharp Bragg peak positioned at $2\theta = 43.4°$ is due to the presence of $AgNO_3$, possibly not removed after sequential washing.

Finally, concerning the Vycor sample, the XRD spectra of pristine and SILP samples are similar (not shown), indicating the absence of crystallization at room temperature.

4. Conclusions

Grafting of ionic liquids onto the pore surface of siliceous supports can be achieved by anchoring of a chloroalkyl trialkoxy silane, which functions as a bridge between the surface and the developed ionic liquid phase. The as synthesized bulk phase (1-methyl-3-(3-trialkoxysilylalkyl) imidazolium hexafluorophosphate) had a lower CO_2 solvation capacity, which was about 87% of that of the commercial [bmim][PF_6^-]. This was attributed to the silyl fragment attached on the alkyl chain of the imidazolium ring which can lead to the loss of organization of the anion [PF_6^-] and the CO_2 about the cation (1-methyl-3-(3-trimethoxysilylpropyl) imidazolium). Despite the lower solvation capacity, both the bulk and surface grafted silylated ionic liquids exhibited excellent CO_2/CO separation capacity.

The pore size of the support is the determinant factor for the extent of pore blockage. Complete coverage of the pore space by the developed [spmim][PF_6^-] is necessary to conclude with a hybrid material exhibiting the gas solvation properties of the bulk ionic liquid and was achieved with the smaller pore size (2.3 nm) MCM-41 support. Complete coverage for the larger pore supports can be further assisted by involving chloroalkyl trialkoxy silanes with bulkier alkyl chains. The tortuosity of the pore structure has a negative effect on the extent of pore blockage due to moderate wetting of the pore channels by the solvent and reactants.

The population of the support's surface silanols may positively affect the amount of the ionic liquid loading and assist in the formation of a continuous ionic liquid phase on the pore surface.

XRD analysis from the SILP sample developed in the MCM-41 support with the larger pore size revealed, for first time, the crystallization behavior of silylated IL at room temperature due to its confinement within the pores. Similarly, based on DSC and XRD analysis, this phase transition was also observed, in a lesser extent, in the case of the confined IL developed on the MCM-41 with the smaller pore size. On the other hand, no evidence for crystallization was concluded for the IL encapsulated in the pores of the Vycor sample.

Acknowledgment. The authors gratefully acknowledge support by the FUSION FP6 and the NEXT-GTL FP7 projects. The assistance of Dr. K. Mergia during the XRD experiments and the XRD analysis is highly appreciated.

Supporting Information Available: The effect of reaction temperature on the silica rehydroxylation, the synthetic procedure for the bulk ionic liquid 1-butyl-3-methylimidazolium hexafluorophosphate ([bmim][PF_6^-]) and the alkoxysilyl-IL 1-methyl-3-(3-triethoxysilylpropyl) imidazolium hexafluorophosphate ([spmim][PF_6^-]), as well as details on the accuracy of the gas absorption measurements. This material is available free of charge via the Internet at http://pubs.acs.org.

References and Notes

(1) Arce, A.; Marchiaro, A.; Rodriguez, O.; Soto, A. *AIChE J.* **2006**, *52*, 2089.
(2) Bourbigou, H. O.; Magna, L. *J. Mol. Catal.* **2002**, *A 182−183*, 419.
(3) Cornils, B.; Herrmann, W. A. *J. Catal.* **2003**, *216*, 23.
(4) Camper, D.; Scovazzo, P.; Koval, C.; Noble, R. *Ind. Eng. Chem. Res.* **2004**, *43*, 3049.
(5) Scovazzo, P.; Camper, D.; Kieft, J.; Poshusta, J.; Koval, C.; Noble, R. *Ind. Eng. Chem. Res.* **2004**, *43*, 6855.
(6) Baltus, R. E.; Culbertson, B. H.; Dai, S.; Luo, H. M.; DePaoli, D. W. *J. Phys. Chem. B* **2004**, *108*, 721.
(7) Zhang, S.; Yuan, X.; Chen, Y.; Zhang, X. *J. Chem. Eng. Data* **2005**, *50*, 1582.
(8) Shiflett, M. B.; Yokozeki, A. *Ind. Eng. Chem. Res.* **2005**, *44*, 4453.
(9) Kuhne, E.; Perez, E.; Witkamp, G. J.; Peters, C. J. *J. Supercrit. Fluids* **2008**, *45*, 27.
(10) Kim, Y. S.; Choi, W. Y.; Jang, J. H.; Yoo, K. P.; Lee, C. S. *Fluid Phase Equilib.* **2005**, *228−229*, 439.
(11) Ohlin, C. A.; Dyson, P. J.; Laurenczy, G. *Chem. Commun.* **2004**, 1070.
(12) Kumelan, J.; Kamps, A. P. S.; Tuma, D.; Maurer, G. *Fluid Phase Equilib.* **2005**, *228*, 229–207.
(13) Jacquemin, J.; Husson, P.; Majer, V.; Costa Gomes Margarida, F. *Fluid Phase Equilib.* **2006**, *240*, 87.
(14) Anthony, J. L.; Maginn, E. J.; Brennecke, J. F. *J. Phys. Chem. B* **2002**, *106*, 7315.
(15) Mehnert, C. P.; Cook, R. A.; Dispenziere, N. C.; Afeworki, M. *J. Am. Chem. Soc.* **2002**, *124*, 12932.
(16) Mehnert, C. P.; Mozeleski, E. J.; Cook, R. A. *Chem. Commun.* **2002**, 3010.
(17) Hagiwara, H.; Sugawara, Y.; Isobe, K.; Hoshi, T.; Suzuki, T. *Org. Lett.* **2004**, *6*, 2325.
(18) Gruttadauria, M.; Riela, S.; Lo Meo, P.; D'Anna, F.; Noto, R. *Tetrahedron Lett.* **2004**, *45*, 6113.
(19) Yang, Y.; Lin, H.; Deng, C.; She, J.; Yuan, Y. *Chem. Lett.* **2005**, *34*, 220.
(20) Shi, F.; Zhang, Q.; Li, D.; Deng, Y. *Chem.−Eur. J.* **2005**, *11*, 5279.
(21) Sasaki, T.; Zhong, C.; Tada, M.; Iwasawa, Y. *Chem. Commun.* **2005**, 2506.
(22) Yamaguchi, K.; Yoshida, C.; Uchida, S.; Mizuno, N. *J. Am. Chem. Soc.* **2005**, *127*, 530.
(23) Romanos, G. E.; Vangeli, O. C.; Stefanopoulos, K. L.; Kouvelos, E. P.; Papageorgiou, S. K.; Favvas, E. P.; Kanellopoulos, N. K. *Microporous Mesoporous Mater.* **2009**, *120*, 53.
(24) Chen, S.; Wu, G.; Sha, M.; Huang, S. *J. Am. Chem. Soc.* **2007**, *129*, 2416.
(25) Yaodong, L.; Zhang, Y.; Wu, G.; Hu, J. *J. Am. Chem. Soc.* **2006**, *128*, 7456.
(26) Holik, M.; Matejkova, B. *J. Chromatogr.* **1981**, *213*, 33.
(27) Landmesser, H.; Kosshck, H.; Storek, W.; Fricke, R. *Solid State Ionics* **1997**, *101−103*, 271.
(28) Benjelloun, M.; Van Der Voort, P.; Cool, P.; Collart, O.; Vansant, E. F. *Phys. Chem. Chem. Phys.* **2001**, *3*, 127.
(29) Kocherbitov, V.; Alfredsson, V. *J. Phys. Chem. C* **2007**, *111* (35), 12906.
(30) Groβmann, F.; Ehwald, V.; du Fresne von Hohenesche, C.; Unger, K. K. *J. Chromatogr., A* **2001**, *910*, 223.
(31) Kumar, D.; Schumacher, K.; du Fresne von Hohenesche, C.; Grun, M.; Unger, K. K. *Colloids Surf., A* **2001**, *187−188*, 109.
(32) Janowski, F.; Heyer, W. *Porose Glaser*; VEB Deutscher Verlag fur Grundstoffindustrie: Leipzig, Germany, 1982.
(33) Kohler, J.; Kirkland, J. J. *J. Chromatogr.* **1987**, *385*, 125.
(34) Beltsios, K.; Charalambopoulou, G.; Romanos, G.; Kanellopoulos, N. *J. Porous Mater.* **1999**, *6* (1), 25.
(35) Choudhury, A. R.; Winterton, N.; Steiner, A.; Cooper, A. I.; Johnson, K. A. *J. Am. Chem. Soc.* **2005**, *127*, 16792.
(36) Xu, W.; Wang, L. M.; Nieman, R. A.; Angell, C. A. *J. Phys. Chem. B* **2003**, *107*, 11749.
(37) Cadena, C.; Anthony, J. L.; Shah, J. K.; Morrow, T. I.; Brennecke, J. F.; Maginn, E. J. *J. Am. Chem. Soc.* **2004**, *126*, 5300.
(38) Yuhuan, C.; Suojiang, Z.; Xiaoliang, Y.; Yanqiang, Z.; Xiangping, Z.; Wenbin, D.; Ryohei, M. *Thermochim. Acta* **2006**, *441*, 42.
(39) Aki Sudhir, N. V. K.; Mellein Berlyn, R.; Saurer Eric, M.; Brennecke Joan, F. *J. Phys. Chem. B* **2004**, *108*, 20355.

JP912205Y